

# Seasonality and scale of the Kerguelen plateau phytoplankton bloom: A remote sensing and modeling analysis of the influence of natural iron fertilization in the Southern Ocean

Mathieu Mongin<sup>a,\*</sup>, Ernesto Molina<sup>a,b</sup>, Thomas W. Trull<sup>a,b,c</sup>

<sup>a</sup>*Antarctic Climate and Ecosystems CRC, Hobart 7001, Australia*

<sup>b</sup>*Institute of Antarctic and Southern Ocean Studies, University of Tasmania, Hobart 7001, Australia*

<sup>c</sup>*CSIRO Marine and Atmospheric Research, Hobart 7001, Australia*

Accepted 12 December 2007

Available online 7 April 2008

## Abstract

The phytoplankton bloom that develops over the Kerguelen plateau following natural input of iron is analysed on a regional and seasonal scale. The relation between chlorophyll, bathymetry, and surface advection fields is not as obvious as it first appears from large-scale annual mean field. The high chlorophyll biomass does not always correspond with the shallowest water, and there are portions of the plateau, which persistently exhibit low chlorophyll. Despite this complex dynamic, a one-dimensional model calibrated for HNLC (high-nutrient low-chlorophyll) region is able to capture the observed increase in chlorophyll by increasing the deep iron concentration. The elemental budget shows similarity in terms of carbon, nitrogen, and silicon but differences in terms of iron with the budget calculated during the mission. This discrepancy either has its origin in the structure of the iron cycling in the model or in the temporal scarcity of data that could only be collected during the summer months. In the model, flexibility of the Fe/C ratio associated with high Fe export and input fluxes prevents high carbon sequestration efficiency. This first insight with remote sensing data and the model allows the validation of some of the key mechanisms of natural iron fertilization and exposes problems that will need to be solved to have a complete biogeochemical diagnostic of this natural iron fertilization.

© 2008 Elsevier Ltd. All rights reserved.

**Keywords:** MODIS; Chlorophyll; KEOPS; Biogeochemical model; Carbon export; Iron fertilization

## 1. Introduction

Artificial iron-fertilization experiments in HNLC waters have shown that iron addition promotes phytoplankton, and especially large-diatom growth (reviewed in De Baar et al., 2005), but have also revealed that the subsequent development and persistence of the bloom depends strongly on the extent of exchange between fertilized and surrounding waters. For example, during SOIREE (Southern Ocean Iron Release Experiment), the artificial addition of iron in the ocean surface led to a chlorophyll patch that persisted much longer than expected (Boyd et al., 2000) due to a favourable combination of stirring, growth, and

diffusion processes (Abraham et al., 2000). In reviewing eight artificial iron experiments, De Baar et al. (2005) also showed that for most of them the dispersion of the phytoplankton bloom was due to horizontal mixing.

The small scale and short duration of these iron fertilization experiments, and thus the enhanced importance of exchange with surrounding waters, have limited their relevance to the assessment of the impact of large scale increased iron availability on Southern Ocean carbon cycling (e.g., Boyd et al., 2002; De Baar et al., 2005). By contrast, KEOPS (Kerguelen Ocean and Plateau compared Study) was designed to address the effects of iron on carbon cycling differently, by examining the area of persistently high phytoplankton biomass that forms over the Kerguelen plateau each year (Fig. 1). Shipboard observations in January–February 2005 revealed that this

\*Corresponding author.

E-mail address: [Mathieu.Mongin@acecrc.org.au](mailto:Mathieu.Mongin@acecrc.org.au) (M. Mongin).

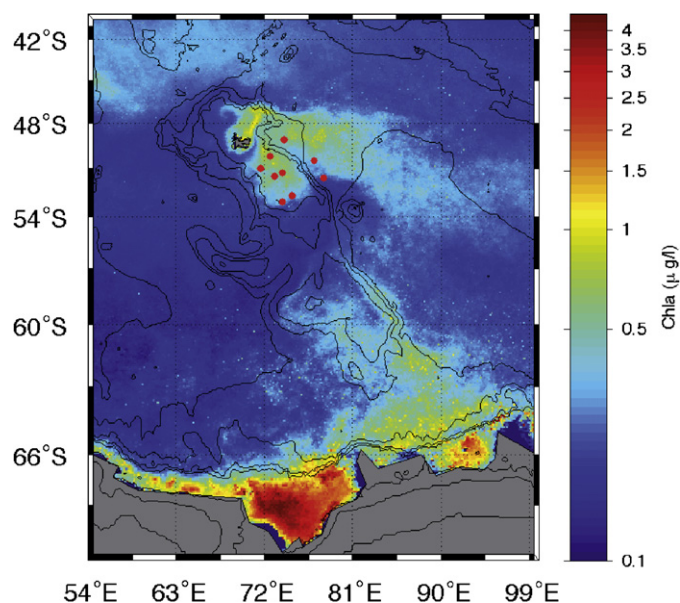


Fig. 1. Map of the Kerguelen plateau area, showing major topography and chlorophyll-*a* climatology (1997–2007) from the MODIS AQUA sensor.

phytoplankton bloom was triggered by enhanced natural iron input from subsurface waters (Blain et al., 2007). The other articles in this special issue use these shipboard observations to examine the distribution and sources of this iron (Blain et al., 2008; Zhang et al., 2008; Van Beek et al., 2008), its availability and uptake by the microbial community (Gerringa et al., 2008; Sarthou et al., 2008) and the subsequent biological response (Mosseri et al., 2008; Obernosterer et al., 2008; Trull et al., 2008; Carlotti et al., 2008; Armand et al., 2008), including the magnitude of carbon dioxide drawdown (Jouandet et al., 2008) and carbon export (Savoie et al., 2008).

In this study we take a larger view, and examine the regional scale and seasonal evolution of the phytoplankton bloom based on satellite images. We then combine this perspective to build a simple model and investigate its response to the observed enhanced iron input. Specifically we:

- Develop a comprehensive description of the Kerguelen plateau bathymetry, chlorophyll-*a* distributions (as estimated from ocean-colour measurements), and surface horizontal advection field (as estimated from satellite altimetry).
- Modify an existing model that has been applied at the nearby KERFIX site in HNLC waters (Mongin et al., 2006; Mongin et al., 2007) to simulate the microbial ecosystem response to increased iron supply.
- Use this model to investigate the seasonal cycle of the bloom, to calculate carbon and iron budgets, and to assess carbon sequestration efficiency, including its dependence on the plasticity of phytoplankton Fe uptake and horizontal dispersion strength.

### 1.1. Context of the KEOPS project

The KEOPS survey during January–February 2005 examined the phytoplankton bloom that forms annually in the vicinity of the Kerguelen plateau. In brief, the Kerguelen plateau is a large area of relatively shallow sea floor in the Indian sector of the Southern Ocean that extends for more than 2200 km southeast from the Kerguelen Islands (49°S, 70°E). Its full extent reaches as far south as the Princess Elizabeth Trough near 63°S, but our interest is focused on the portion of the plateau north of the Fawn Trough, between and to the east of the Kerguelen and Heard Islands (Fig. 1). From here on we refer to this region as “the plateau”.

High-energy internal tidal waves that interact with the bathymetry enhance the vertical eddy diffusivity above the plateau, and hence the supply of subsurface iron and other nutrients (Park et al., 2008a). This supply from below appears to be the main source of iron to fuel the phytoplankton bloom, with negligible aeolian iron dust fluxes from the Kerguelen desert (Blain et al., 2007).

Despite the high primary production and standing stock of chlorophyll in the Kerguelen bloom, surface-water nitrate depletion was insufficient to limit phytoplankton production, although near complete depletion of silicic acid did occur (Blain et al., 2007; Mosseri et al., 2008). Similar decoupling of the Si and N cycles was observed during experimental iron-fertilization experiments (Boyd et al., 2004), and also resembles the general much larger depletion of silicic acid than nitrate in surface waters from south to north across the Southern Ocean (Trull et al., 2001a).

Both on and off the plateau, the planktonic ecosystem structure was dominated by large diatoms and large copepods (Armand et al., 2008; Carlotti et al., 2008). Bacterial activity was elevated over the plateau (Obernosterer et al., 2008) and the utilisation of new nitrogen by phytoplankton also appeared to be greater (Mosseri et al., 2008; Trull et al., 2008). At the time of the KEOPS survey, particulate carbon export over the plateau was approximately twice that of surrounding waters (Blain et al., 2007; Savoie et al., 2008). Based on surface dissolved inorganic carbon concentrations a similar enhancement seems to persist over the full season (Blain et al., 2007; Jouandet et al., 2008).

### 1.2. Regional description

Based on mean annual ocean colour (Fig. 1) and animations of the seasonal cycle (available at <http://staff.acecrc.org.au/~mmongin/>), the satellite-derived surface chlorophyll-*a* (SCHL) distribution over the region can be separated into four regimes:

- North of the SAF (subantarctic front), in subtropical waters (40°S–45°S) the SCHL is usually low (max of  $1.5 \text{ mg Chl } a \text{ m}^{-3}$ ) and develops late in the season (January).

- (ii) In the southeast section, an area of elevated SCHL forms near the Banzare bank, probably associated with meandering of the Southern Antarctic Circumpolar Current (ACC) Front.
- (iii) In an east–west band just to the north of Kerguelen Island, there is an area of high SCHL associated with mesoscale eddies within the SAF (Moore and Abbott, 2002). This activity often merges with the coastal plume of SCHL around Kerguelen Island and sometimes extends southeast to merge with the high SCHL over and to the east of the plateau.
- (iv) The last pattern is the bloom studied during the KEOPS project, over shallow waters (1000 m) between Kerguelen and Heard Islands. This bloom starts sooner (November) than in waters to the north (January, for 40°–45°S). It has a round shape and seems to extend from a central point within the plateau.

### 1.2.1. Bathymetry of the Kerguelen Plateau

Most of the area of study (49°S–53.5°S 69°E–78°E) is shallower than 1000 m (Fig. 2). In addition to Kerguelen and Heard Islands, there are three bathymetric features that seem relevant to the spatial distribution of SCHL:

- (i) the relatively deep (~650 m) trough that runs east–west across the plateau just south of Kerguelen Island, (ii) the central area of relatively shallow bathymetry (~500 m) which is round in shape and includes five shallower seamounts, and (iii) the relatively shallow (300–500 m deep) northern extension of the Williams Ridge at the far southeastern edge of the plateau, which is separated from the central plateau by a northwest–southeast trough of deeper (~600 m) waters. For simplicity, we refer to these features hereafter as (i) the Polar Front trough, (ii) the central plateau, and (iii) the southeastern trough and ridge.

### 1.2.2. General circulation

The Kerguelen plateau acts as a barrier and forces the large-scale flow of the ACC to divide. Approximately  $\frac{2}{3}$  of the transport goes north of Kerguelen Island (Park et al., 2008b; McCartney and Donohue, 2007) and exhibits strong meandering and eddy activity (Stammer, 1998; Moore and Abbott, 2000). The remaining flow passes through the Fawn Trough where it divides the northern and southern portions of the plateau (Park et al., 2008b; McCartney and Donohue, 2007). Farther east, the flow through the Fawn Trough turns back north and west along contours of bathymetry east of the Williams Ridge.

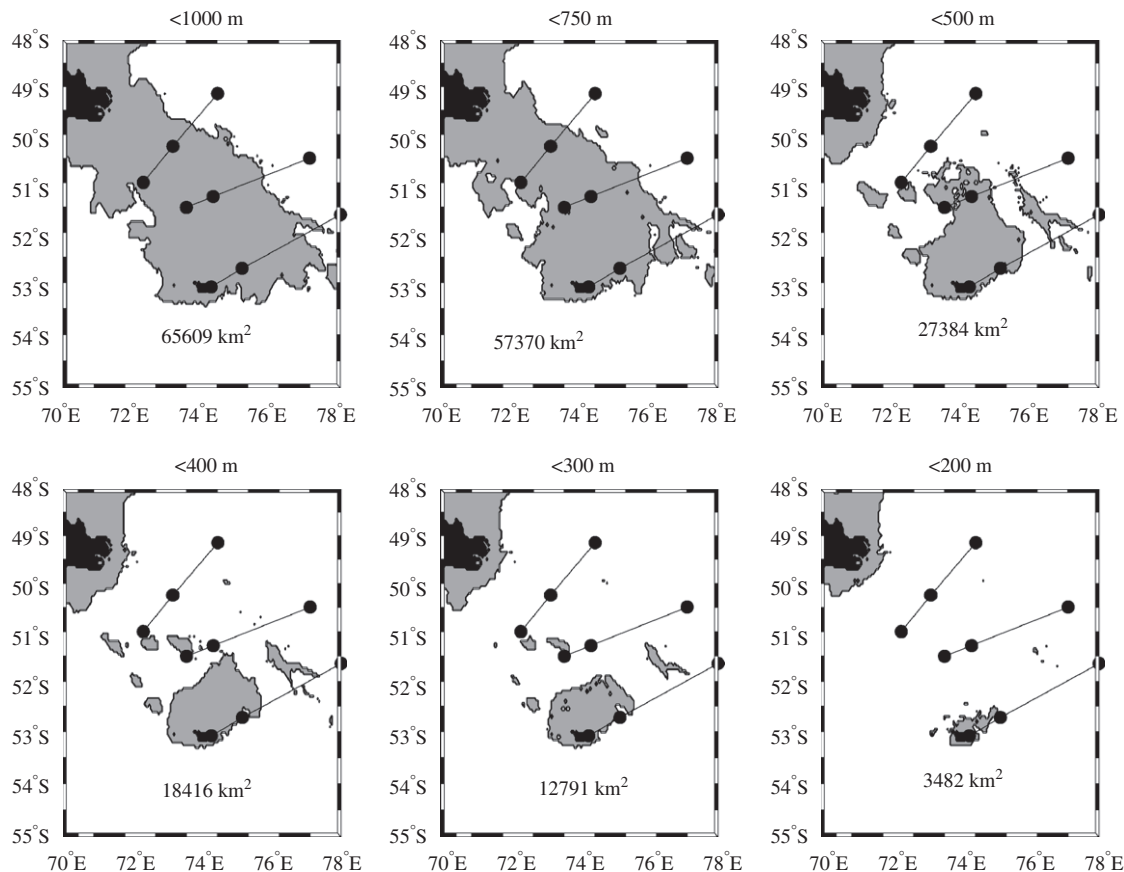


Fig. 2. Bathymetry and area of the Kerguelen plateau (in km<sup>2</sup> based on different depths (1000, 750, 500, 400, 300, and 200 m). Lines represent the three transects surveyed during KEOPS.

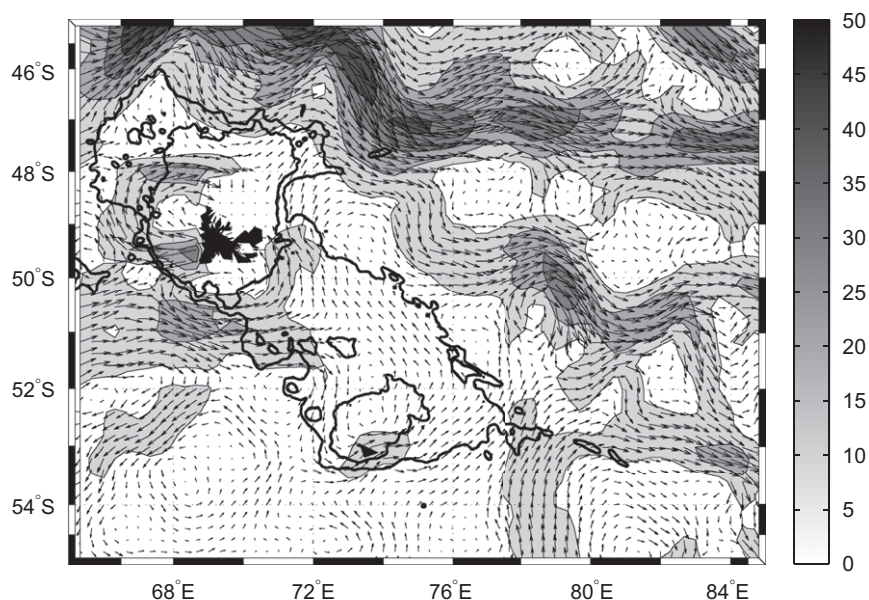


Fig. 3. Summer mean (November–February) of the absolute geostrophic velocity ( $\text{m s}^{-1}$ ) derived from sea-surface elevation (based on the combined AVISO product of Jason-1 Topex Poseidon and Envisat). The altimeter products were produced by Ssalto/Duacs and distributed by AVISO, with support from CNES. Also shown are the 300- and 500-m isobaths.

This division of the ACC leads to relatively sluggish circulation across the plateau. Some waters enter our study region from south of Heard Island along contours of bathymetry and flow north and back west across the plateau; others enter from the west, north of Heard Island, flow northward and exit to the east in the branch of the Polar Front (Park et al., 2008b). Based on CTD and ADCP observations made during the KEOPS cruise surface velocities are weak ( $2\text{--}8 \text{ cm s}^{-1}$ ). Altimetry-based geostrophic fields (Fig. 3) suggest a similar pattern of small and generally northward flow over the plateau. The stronger velocity signal within the southeastern trough between the central plateau and the southeastern ridge is also visible as well as the persistent flow of waters through the Polar Front trough just south of Kerguelen Island that separates Kerguelen Island coastal waters from the central plateau. More detailed discussion of the circulation is presented in Park et al. (2008b).

### 1.2.3. Details of the phytoplankton bloom development and shape

Links between the bathymetry and the SCHL distributions have already been studied in the Southern Ocean (Moore and Abbott, 2000; Pollard and Read, 2001; Sokolov and Rintoul, 2007) including the Kerguelen zone (Pollard et al., 2002). In this study, we address those links in the context of the KEOPS project by examining higher resolution images and developing a comprehensive description of the distribution of SCHL on and around the central plateau.

To develop our estimates of the spatial distribution of SCHL concentrations (in  $\text{mg m}^{-3}$ ) we used 8-day composites images at 4-km resolution from the moderate resolution imaging spectroradiometer (MODIS/AQUA)

produced by NASA. Because of high cloud cover, only 18 such images could be exploited for the 2004/2005 season (cloud coverage equal or smaller than 30%).

Fig. 4 presents four of these images. Focusing on the central bloom, phytoplankton biomass begins to develop over the plateau in November above the 500–1000 m depth zone. At the end of November the central bloom occupied most of the area between the two islands with a relatively round shape. By December the bloom had started to fade, and in late January it shrank back to occupy only the part of the plateau between the two islands (constrained by the 500 m isobath). The elevated SCHL is usually located in relatively deep waters (300–500 m) rather than the shallowest waters (0–200 m), possibly as a result of higher currents within these troughs.

The SCHL does extend off the plateau to some extent, especially to the northeast and southeast. This could reflect the interaction of northward advection from the plateau with the southward meandering of the SAF. A thin band of low SCHL is almost always present in the Polar Front trough just south of Kerguelen Island ( $40^\circ\text{S } 70^\circ\text{E}$ ). This is an important feature for the evaluation of hypotheses about the processes that fuel the bloom over the plateau, as it suggests that direct inputs from Kerguelen Island are probably carried away from the central plateau.

The MODIS-derived SCHL time series (Fig. 5) shows a typical polar seasonality with a single peak in early summer rather than the bimodal early spring and early autumn peaks typical of subantarctic waters (Trull et al., 2001b). It should be noted that despite the overall good quality of the MODIS colour sensor and calibration process, unreliable pixels are still present especially during winter, including high values (up to  $>4 \text{ mg Chl m}^{-3}$ ) reported in August and November.

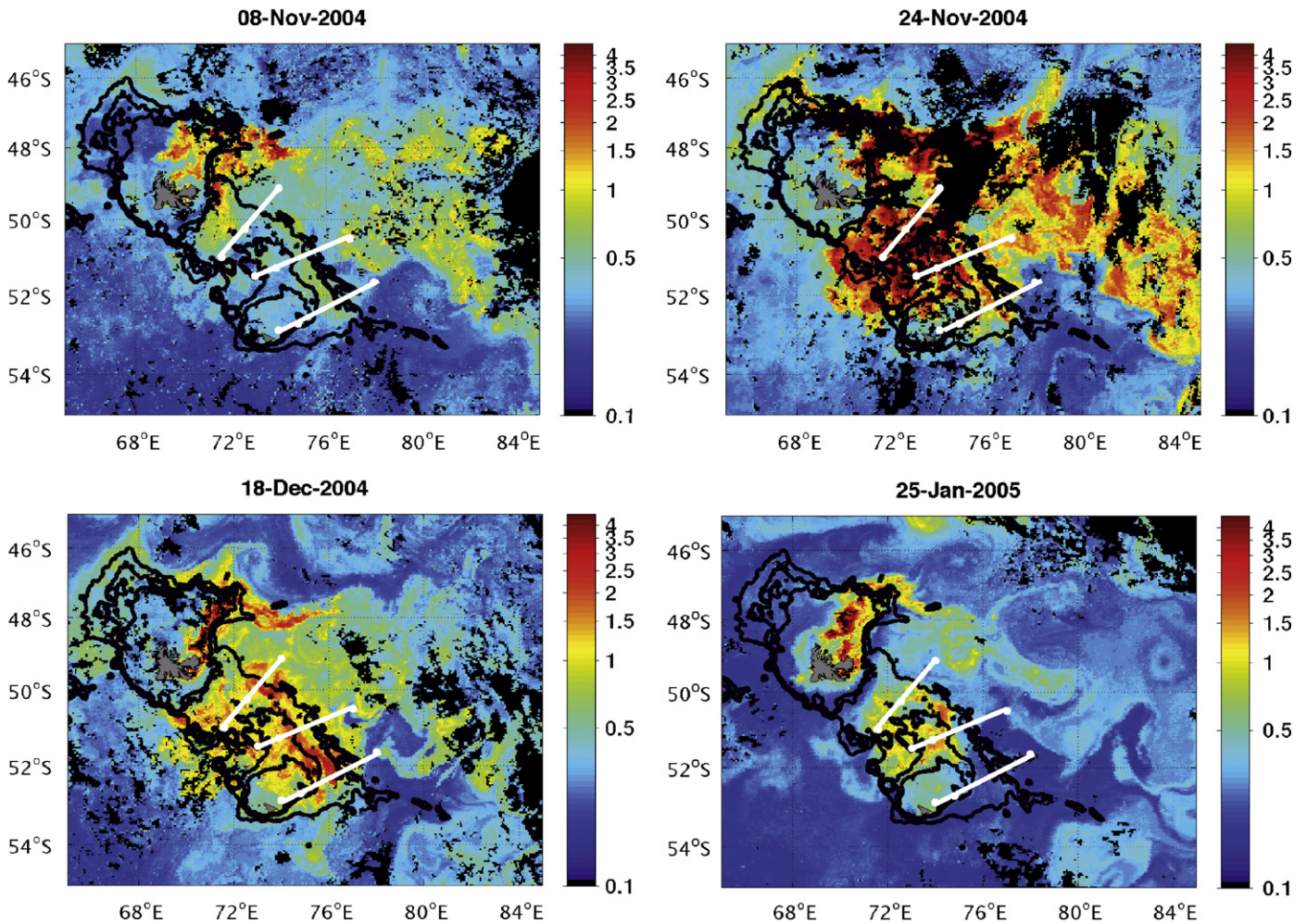


Fig. 4. MODIS AQUA SCHL images during the bloom period (for dates with minimal cloud coverage). Contours show the bathymetry (300, 500, and 1000 m isobaths). KEOPS transects are shown as lines.

## 2. Biogeochemical simulation

Because our aim is to simulate the broad characteristics of the central plateau bloom, and because dispersion above the plateau is low (compared to the surrounding area), we decided to use a simple purely diffusive dispersion model coupled with an existing biogeochemical module. We therefore develop a two-dimensional (horizontal) bulk mixed-layer model using a one-dimensional model calibrated at the nearby HNLC KERFIX time series site (Mongin et al., 2006). The biogeochemical parameterization is taken from the KERFIX model and thus provides an ideal simulation to address whether an HNLC model can simulate the Kerguelen plateau bloom by just increasing the DFe concentration below the mixed layer.

### 2.1. Model description

Daily mixed-layer depths are taken from a turbulent kinetic energy one-dimensional (80 vertical levels) model (Mongin et al., 2006). This vertical mixing represents the mean forcing for the 1989–1995 period, so that our

simulation is for an “average” bloom rather than specific to the 2004–2005 KEOPS observation period. We also assume that vertical mixing is uniform across the model domain (above and outside the fertilization zone).

The new model considers the mixed layer (MLD) and a deep nutrient reservoir underneath (no bathymetry or interaction with the ocean bottom). Nutrient entrainment (from the deep reservoir toward the mixed layer) is simulated using the following daily variation of the MLD scheme (based on Moore et al., 2002):

$$\begin{aligned} \text{MLD}^{t-1} < \text{MLD}^t \dots & \left\{ Fe_1 = \frac{(\text{MLD}^{t-1} - \text{MLD}^t)}{\text{MLD}^t} \right. \\ & \left. \times (Fe_{\text{deep}} - Fe_{\text{MLD}}) \right\}, \\ \text{MLD}^{t-1} > \text{MLD}^t \dots & \{ Fe_1 = 0 \}, \end{aligned} \quad (1)$$

where MLD is the mixed-layer depth,  $Fe_1$  is the entrainment function, and  $Fe_{\text{deep}}$  and  $Fe_{\text{MLD}}$  are dissolved iron concentrations below and within the mixed layer, respectively. Analogous function are used for  $\text{NO}_3^-$  and  $\text{Si}(\text{OH})_4$  entrainment. The deep reservoir concentration of nutrient

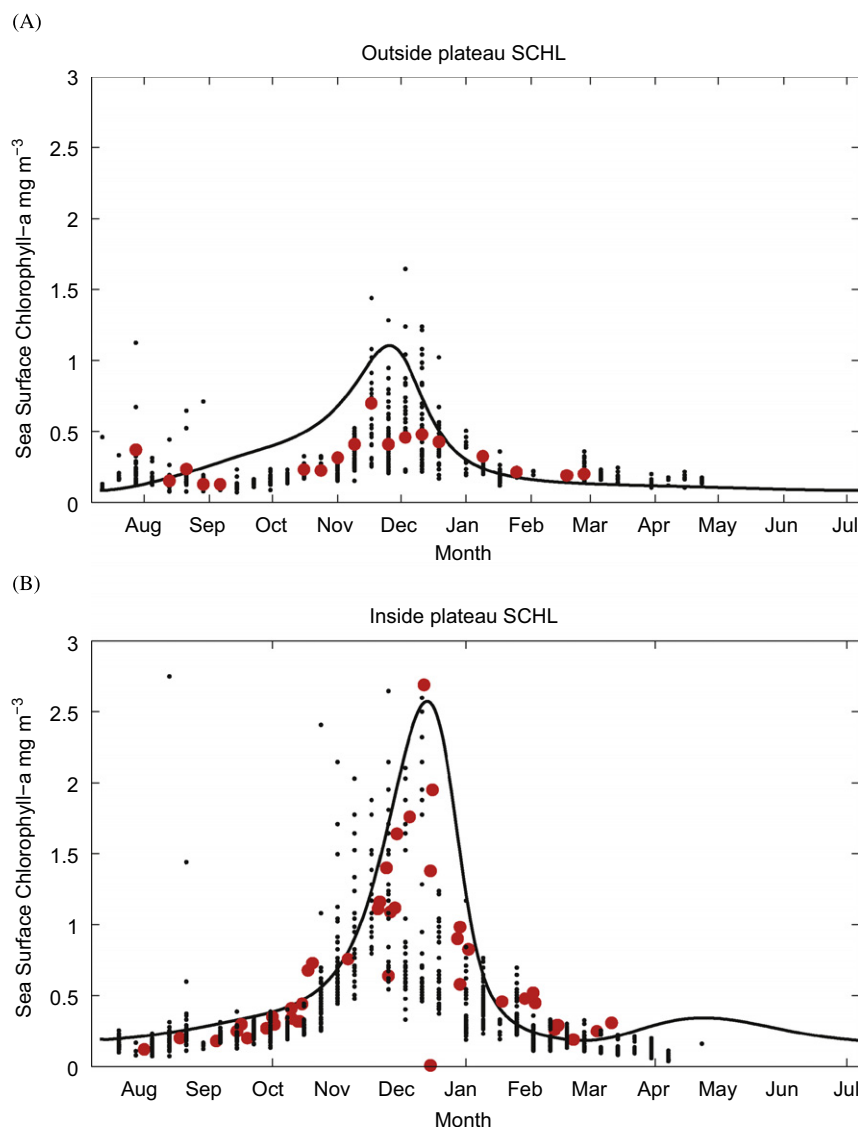


Fig. 5. SCHL seasonal time series above (A) and outside (B) the plateau for the model (plain lines for  $K_x = 0 \text{ m}^2 \text{ s}^{-1}$ ), and from the MODIS-AQUA observations (dots) along meridional transects at  $72^\circ \text{E}$  and  $78^\circ \text{E}$  (see Section 2.2) and for the KEOPS reference station, C11 and A3 (red dots).

is also taken from the one-dimensional model. Detritus (in carbon, nitrogen, silicon, and iron units) is allowed to sink between the two boxes.

This bulk vertical model was run on a  $400 \times 400 \text{ km}^2$  horizontal grid (20-km resolution) representing the area over and surrounding the Kerguelen plateau. Physical dispersion between horizontal boxes is treated using an upstream diffusive scheme and constant eddy diffusivity  $K_x$ . For the base simulations we used a  $K_x$  of  $0 \text{ m}^2 \text{ s}^{-1}$  (purely vertical case) and  $250 \text{ m}^2 \text{ s}^{-1}$  (best estimate based on global maps of altimetry from Stammer, 1998). We then explored the sensitivity to higher  $K_x$  values of 500 and  $1000 \text{ m}^2 \text{ s}^{-1}$  such as those occurring further north closer to the SAF (Stammer, 1998). Photosynthetically available radiation (PAR) is assumed to be 45% of the short-wave radiation and is averaged over the MLD using an absorption coefficient that depends on water and chlorophyll concentration (Lancelot et al., 1991).

The fertilization zone is defined in the model as the central  $6 \times 6$  ( $14,400 \text{ km}^2$ ) set of grid cells (corresponding to the area occupied by the 300 m isobath  $12,791 \text{ km}^2$ , see Figs. 2 and 6). Within those cells, the deep (below the mixed layer) iron concentration is increased by a factor 3 to reflect the higher DFe values observed during KEOPS (Blain et al., 2007).

Coupled to this basic physical frame, we used a slightly modified version of the Mongin et al. (2006) biogeochemical model that includes carbon, nitrogen, silicon, and iron cycling. The model incorporates one phytoplankton class (diatoms), two-size classes of zooplankton (micro- and mesozooplankton), heterotrophic bacteria, two detritus pools (large and small), and two dissolved organic matter pools (labile and semi-labile). Each of the nutrient elements is tracked in each of these pools. Importantly, the model allows uptake of  $\text{NO}_3^-$ ,  $\text{NH}_4^+$ ,  $\text{Si(OH)}_4$ , biologically available iron  $\text{Fe}_B$  (which is taken to be equivalent to

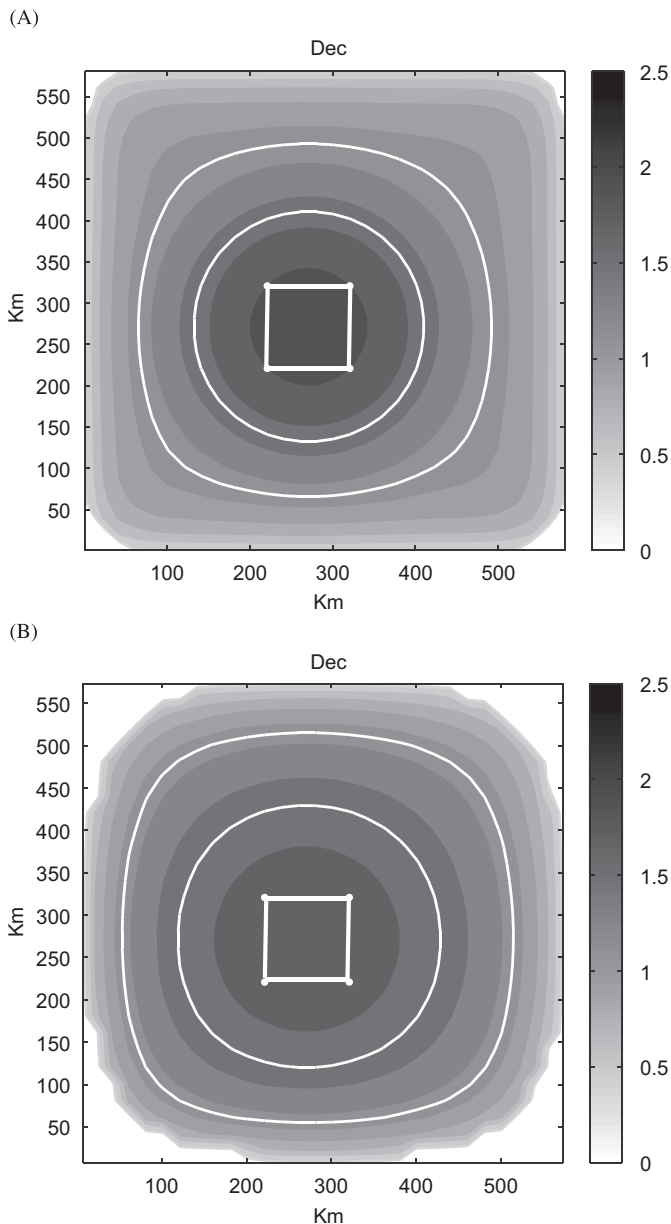


Fig. 6. Surface SCHL ( $\text{mg Chla m}^{-3}$ ) simulated in the model in mid-December. (A) In the  $K_x = 250 \text{ m}^2 \text{ s}^{-1}$  and (B)  $K_x = 1000 \text{ m}^2 \text{ s}^{-1}$  version of the model. White square in the centre outline the infusional zone. Also shown are the 1.8 and 1.5  $\text{mg Chla}$  contours.

dissolved Fe, DFe), and photosynthetic fixation of C to be independent of each other within a constrained range of elemental ratios as proposed by the Droop (1974) cell quota model. When phytoplankton Fe/C ratio reaches low values ( $< 10^{-4} \text{ mol/mol}$ ), photosynthetic efficiency ( $\alpha$ ) and maximum rate of  $\text{NO}_3^-$  uptake decrease (following Droop's model) and reach zero at the lowest cellular Fe/C ratio permitted ( $1.5 \times 10^{-6} \text{ mol/mol}$ ). When  $\text{Fe}_B$  is abundant in the environment, enhanced  $\text{Fe}_B$  uptake can elevate the cellular Fe/C ratio up to a maximum of  $2 \times 10^{-3}$ , although above a Fe/C of  $2 \times 10^{-4} \text{ mol/mol}$   $\text{Fe}_B$  uptake slows down.

This plasticity of the ratio of Fe/C uptake by phytoplankton is a key aspect of our model, in that it allows the

enhanced supply of  $\text{Fe}_B$  over the plateau to be taken up without necessarily requiring a large accumulation of phytoplankton biomass (carbon or nitrogen uptake). As such, nutrient uptake (and photosynthesis) is not only controlled by extracellular concentrations (or light intensity for photosynthesis), but also by the C/N/Si/Fe ratios within the phytoplankton cell. This aspect distinguishes the Fe uptake from a formulation such as might be used for extra-cellular scavenging of iron.

Grazing and other mortality convert diatoms into detrital particulate matter. We assume that Fe is ingested along with organic matter but that the grazers assimilate negligible Fe. Removal of phytoplankton Fe by grazing is calculated as the ingestion rate of phytoplankton in carbon multiplied by the Fe/C ratio of phytoplankton. All Fe ingested by zooplankton is rejected into the detritus pool as faecal pellets, and the model tracks the Fe/C, Fe/N, and Fe/Si ratios of the detritus. The specific rates of both N regeneration and Fe regeneration from detritus were set to  $0.05 \text{ d}^{-1}$ . A full mathematical formulation of these processes is presented in Mongin et al. (2003, 2006).

## 2.2. Biogeochemical simulation of the bloom seasonality

The non-dispersive version of the model ( $K_x = 0 \text{ m s}^{-1}$ ) simulates reasonably well the seasonal cycles of mixed-layer chlorophyll (taken as equivalent to SCHL) over and adjacent to the plateau, as shown by comparison of model and MODIS SCHL along meridional transects at  $72^\circ \text{E}$  ( $49.5^\circ \text{S}$ – $53^\circ \text{S}$ ) for the fertilization zone and  $78^\circ \text{E}$  ( $49.5^\circ \text{S}$ – $53^\circ \text{S}$ ) for the HNLC conditions (Fig. 5). We used meridional transects to allow a better comparison of the model and data. This reduces biases from clouds and sub-mesoscale patterns in the observed SCHL that can arise when using a single location. The bloom transect along  $72^\circ \text{E}$  gives a very similar signal to the one obtained by Blain et al. (2007) at the reference bloom station A3. The off-plateau  $78^\circ \text{E}$  transect yields a small seasonal bloom for the off-plateau conditions that is very similar to the seasonal cycle observed in KERFIX data (Fiala et al., 1998) where the base 1-D model was calibrated (Mongin et al., 2006; Mongin et al., 2007). This small seasonal bloom differs from the negligible bloom observed at the KEOPS HNLC reference station C11 (Fig. 5, Blain et al., 2007). As discussed below in Section 2.3, this difference may reflect greater iron availability at KERFIX and along  $78^\circ \text{E}$  than at C11, or possibly other factors such as differences in surface-water temperature or the seasonality of stratification (C11 exhibited colder surface temperatures than A3 or KERFIX during KEOPS).

In the model as in the observations, the bloom starts in early November and reaches its maximum by mid-December ( $1.1 \text{ mg m}^{-3}$  SCHL outside and  $2.5 \text{ mg m}^{-3}$  inside the plateau). By late February the SCHL drops back down to less than  $0.5 \text{ mg m}^{-3}$  in both areas. The most important result is that the model reproduces the observed

change between the fertilization zone and the HNLC regime in term of SCHL.

The simulated SCHL maximum over the plateau takes place later ( $\sim 3$  weeks) than off plateau (Fig. 5). Comparing the MODIS SCHL observations on and off the plateau (compare the two panels of Fig. 6) reveals that this early development is a real aspect of the plateau bloom and not just a mismatch between the model and the observations. The origin of this earlier seasonal SCHL maximum over the plateau is not known. It could represent differences in water-column stratification or physical forcing—differences that are not simulated by our model.

A diffusion coefficient of  $250 \text{ m s}^{-1}$  causes the bloom to cover an area  $\sim 4$  times larger than the infusion zone (using a threshold SCHL of 1.9, Fig. 6A) that is about the same ratio as in the observations if we assume that the real infusion zone is also constrained by the 300 m isobath. As expected when the coefficient of diffusion increases, the horizontal gradient of SCHL between the infusion zone and the HNLC zone is smaller. Thus the two-dimensional model ( $K_x = 250 \text{ m s}^{-1}$ ) produces a higher seasonal maximum in SCHL ( $\sim 1.6 \text{ mg m}^{-3}$ ) for the off-plateau meridional transect than is simulated by the one-dimensional model ( $K_x = 0 \text{ m s}^{-1}$ ), or was estimated for the KEOPS C11 HNLC reference station at the far southeastern edge of the study region ( $\sim 0.5 \text{ mg m}^{-3}$ ). Above the infusion zone, the SCHL stays the same at  $2.5 \text{ mg m}^{-3}$ . This behaviour is specific to the  $K_x$  value of  $250 \text{ m}^2 \text{ s}^{-1}$ , which is sufficient to disperse Fe and chlorophyll concentrations from the plateau to adjacent water masses. Using a  $K_x$  of  $1000 \text{ m}^2 \text{ s}^{-1}$  further homogenizes the bloom (Fig. 6B).

### 2.3. Simulated seasonal cycles of iron and nutrient concentrations

Because of the limited nature of the two-dimensional dispersive model, including uncertainties in the dispersion rate, and its relatively low effect on the simulated SCHL maximum (between the  $K_x = 0$  and  $250 \text{ m s}^{-1}$  simulations), we focus on the simulated seasonal cycles obtained with the non-dispersive model. The maximum MLD of  $\sim 275 \text{ m}$  as determined from the one-dimensional turbulent kinetic-energy model occurs in early spring, and is followed by steady shallowing throughout October and November to a fairly steady summer MLD of  $\sim 80 \text{ m}$ , consistent with the KEOPS observations (Blain et al., 2007). Outside the plateau, DFe reaches a seasonal maximum of  $0.25 \text{ nM}$  (Fig. 7) in surface in late winter (August), but is quickly reduced by phytoplankton uptake to less than  $0.05 \text{ nM}$  by early September, where it remains until the following winter. Over the plateau, the subsurface DFe concentration is specified to be three times the off-plateau values to simulate iron enrichment; this leads to a late winter mixed-layer DFe maximum of  $0.6 \text{ nM}$ , which is also reduced to  $0.05 \text{ nM}$  in summer.

The winter maximum iron concentrations in the model are larger than values estimated from the KEOPS

observations. Blain et al. (2007) estimated a winter mixed-layer DFe of  $0.15 \text{ nM}$  at A3 (plateau reference site) and  $0.086 \text{ nM}$  at C11 (HNLC off-plateau reference site) based on DFe concentrations measured in late summer at the subsurface temperature as an indicator of the remnant winter water. The higher concentrations in the model are closer to the values observed at depth over the plateau (Blain et al., 2007). The model summer DFe concentrations are comparable to, though somewhat less than the values observed during KEOPS (DFe of  $0.086 \text{ nM}$  at both A3 and  $0.072 \text{ nM}$  at C11 in January; Blain et al., 2007).

In the model, the strong decrease in mixed-layer DFe early in the year occurs because of the flexible Fe/C stoichiometry (which also produces the bimodal mixed-layer DFe winter maximum as a result of light-Fe limitation interactions and the Droop model formulation). This contrasts with the assumption of a seasonally steady drawdown of DFe (and DIC) in the budgets presented by Blain et al. (2007) and Jouandet et al. (2008), and leads to continued strong transfer of DFe from the subsurface to the mixed layer as DFe gets taken up by phytoplankton without growth.

Modelled phytoplankton iron concentrations over the plateau peak at slightly above  $2 \text{ nM}$  in early October (but only  $0.2 \text{ nM}$  outside the plateau) and then decline strongly in response to DFe depletion. The sum of detrital and phytoplankton iron reaches  $\sim 3.5 \text{ nM}$  and thus greatly exceeds the DFe pool in spring and early summer before dropping back below DFe levels in early January. The on-plateau particulate iron concentrations in the model exceed the off-plateau values by  $\sim 8$ -fold, while DFe concentrations are only 2-fold higher. Thus throughout this period, biological forms of iron dominate the mixed-layer stock, and its recycling provides the main source of DFe for further phytoplankton uptake. This is consistent with strong iron regeneration observed during KEOPS (Sarhou et al., 2008).

While the iron cycle in our model emphasizes early uptake and stronger seasonal amplitude in DFe than inferred from the KEOPS observations, simulated macronutrients concentrations stay close to the observations. The summer residual concentration of  $\text{NO}_3^-$  is  $26 \mu\text{M}$  (outside plateau) and  $23 \mu\text{M}$  (inside plateau), and  $\text{Si(OH)}_4$  decreases to  $10 \mu\text{M}$  (outside) and approaches depletion at  $2 \mu\text{M}$  inside the plateau. This moderate macro-element cycle response, in comparison to that of iron, occurs because the phytoplankton reaction to increased supply of DFe is quasi-exponential in terms of cellular iron quota, but due to the plasticity of the Fe/C ratio and its effect on photosynthesis nitrate and silicic acid uptake, the phytoplankton response in term of carbon biomass and Chl *a* is much smaller ( $\sim$  factor 2 increase). The Fe/C cell quota measured during KEOPS in February were  $\sim 4.5 \mu\text{mol/mol}$  (Sarhou et al., 2008), close to the value obtained in the model for the same period ( $1.7 \mu\text{mol/mol}$ ). This shows that in January in the model, phytoplankton cells are already growth limited by iron. On the seasonal scale, the Fe/C

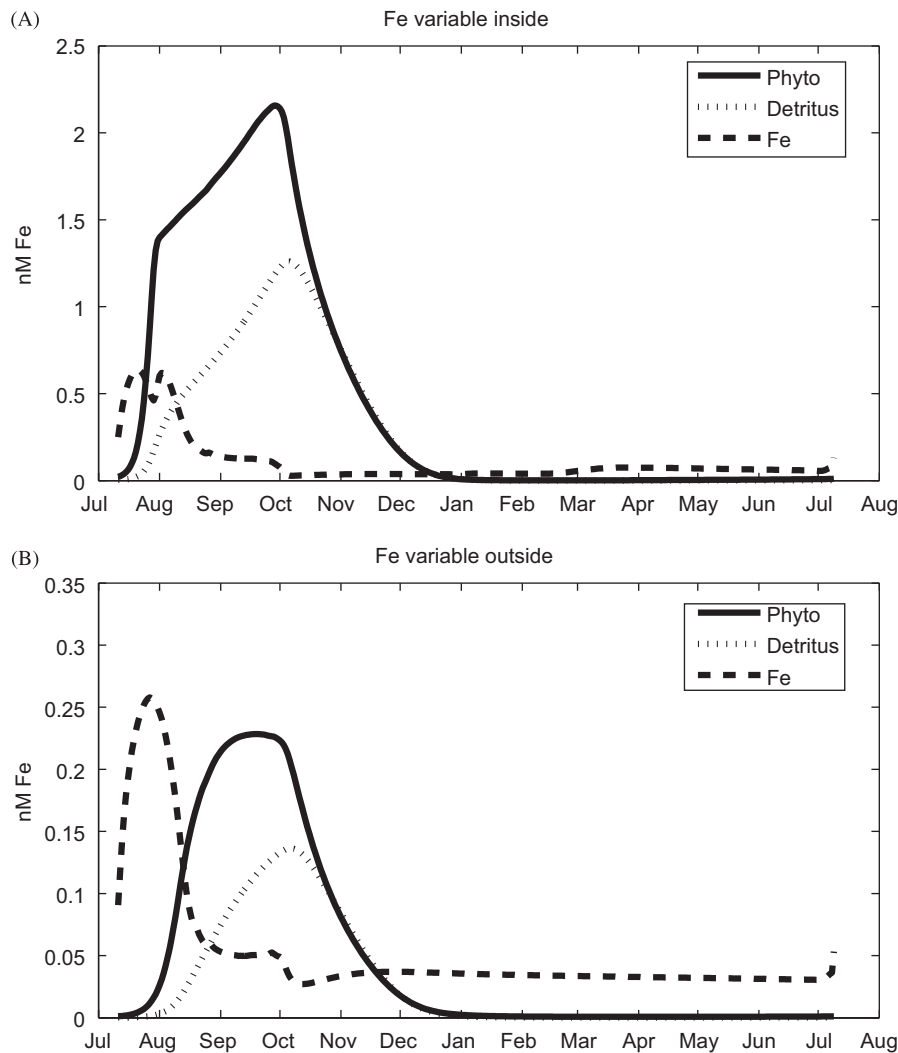


Fig. 7. Seasonal evolution of the model ( $K_x = 0 \text{ m}^2 \text{ s}^{-1}$ ) iron variables (phytoplankton iron, detrital iron, and dissolved bioavailable iron); (A) inside and (B) outside the infusio zone.

ratio of the phytoplankton cells is highly variable in the model, with maximum values attained in September–October ( $1800 \mu\text{mol}/\text{mol}$  inside and  $200 \mu\text{mol}/\text{mol}$  outside).

#### 2.4. Carbon and iron budgets and the calculation of the C/Fe sequestration efficiency

Annual budgets simulated by the non-dispersive model ( $K_x = 0$ ) are presented in Table 1. Inside the plateau, the simulated annual primary production is  $8.6 \text{ mol C m}^{-2} \text{ yr}^{-1}$ , thus 1.7 times higher than outside the plateau. These results are comparable with the value computed by Jouandet et al. (2008), a 3-fold increase between in and off plateau,  $6.3 \pm 2.1$  and  $1.8 \pm 0.1 \text{ mol C m}^{-2} \text{ yr}^{-1}$ . The model maximum daily uptake of DIC is  $80$  (outside) and  $110 \text{ mmol C m}^{-2} \text{ d}^{-1}$  (inside), slightly higher than the  $92.8 \pm 36.6 \text{ mmol m}^{-2} \text{ d}^{-1}$  calculated at the central bloom site A3 during KEOPS (Jouandet et al., 2008). The exported POC fluxes calculated using a seasonal carbon budget (Jouandet et al., 2008)

are  $5.1 \pm 1.9$  (plateau) and  $1.7 \pm 0.4 \text{ mol C m}^{-2} \text{ yr}^{-1}$  (off-plateau). These are larger than the model values of  $2.1$  (plateau) and  $1.2 \text{ mol C m}^{-2}$  (off-plateau).  $^{234}\text{Th}$ -based downwards fluxes of POC during the KEOPS campaign were lower than those suggested from the seasonal carbon budget and closer to the model (Savoie et al., 2008). Overall, the model carbon fluxes were similar to the various observations within about a factor of 2.

Comparison of iron budgets from the model with those from KEOPS and other observations reveals differences that emphasize uncertainties in iron biogeochemistry. The main discrepancy between the model and the budget from Blain et al. (2007, 2008) is the seasonal vertical input of Fe to the mixed layer. Based on a vertical diffusivity in the order of  $10^{-4} \text{ m}^2 \text{ s}^{-1}$ , they calculated a vertical iron supply to the mixed layer of  $6670$  and  $1500 \text{ nmol m}^{-2}$  (A3 bloom and C11 HNLC sites, respectively). In the model the annual vertical iron supply to the mixed layer was  $1.2 \times 10^5 \text{ nmol m}^{-2}$  and  $1.4 \times 10^6 \text{ nmol m}^{-2}$  (off and

Table 1  
Comparison of annual mixed-layer carbon and iron fluxes simulated by the model with KEOPS observations

	Units	Model		KEOPS		Ratio in/out	
		Off plateau	In plateau	Off plateau	In plateau	Model	KEOPS
<b>Uptake</b>							
Iron	$\mu\text{mol m}^{-2}\text{yr}^{-1}$	<b>2.3E+02</b>	<b>2.3E+03</b>	9.5E-01	4.7E+00	1.0E+01	4.0E+00
DIC	$\text{mol m}^{-2}\text{yr}^{-1}$	<b>5.4E+00</b>	<b>8.6E+00</b>	1.5E+00	4.4E+00	1.5E+00	2.9E+00
<b>Remineralization</b>							
Iron	$\mu\text{mol m}^{-2}\text{yr}^{-1}$	<b>9.7E+01</b>	<b>9.4E+02</b>				
<b>Export (mixed layer)</b>							
Iron	$\mu\text{mol m}^{-2}\text{yr}^{-1}$	<b>1.2E+02</b>	<b>1.2E+03</b>				
Carbon	$\text{mol m}^{-2}\text{yr}^{-1}$	<b>1.2E+00</b>	<b>2.1E+00</b>	1.7E+00	5.0E+00	1.9E+00	2.9E+00
Export/uptake ratio Fe	mol/mol	<b>5.0E-01</b>	<b>5.0E-01</b>			4.0E-01	4.0E-01
Export/uptake ratio C	mol/mol	<b>2.0E-01</b>	<b>2.0E-01</b>			2.0E-01	2.0E-01
<b>Iron/carbon export fluxes ratio</b>							
Uptake	$\mu\text{mol Fe/mol C}$	<b>4.2E+01</b>	<b>2.7E+02</b>	4.2E+01	2.9E+02		
Export	$\mu\text{mol Fe/mol C}$	<b>9.8E+01</b>	<b>5.8E+02</b>	1.0E+02	5.7E+02		
Iron input (mixing)	$\mu\text{mol m}^{-2}\text{yr}^{-1}$	<b>1.2E+02</b>	<b>1.4E+03</b>	1.5E+00	6.6E+00	1.1E+01	4.4E+00
<b>Carbon sequestration efficiency</b>							
C export/Fe input	mol/mol	<b>9.6E+03</b>	<b>1.5E+03</b>	1.5E+06	9.9E+05		
DIC uptake/Fe input	mol/mol	<b>4.4E+04</b>	<b>6.3E+03</b>	3.9E+04	5.5E+03		
C export excess/Fe input excess	mol/mol		<b>7.0E+02</b>		7.0E+04		

on-plateau, respectively), that is, one to two orders of magnitude larger (Table 1). However, the difference in the seasonal supply of Fe between in and off plateau conditions is less severe ( $\sim 4.4$  times in the data,  $\sim 11$  times in the model).

The high iron input to the mixed layer derives from three sources in the model:

- (i) our assumption that mixed-layer DFe concentrations can reach 0.6 nM over the plateau in winter, i.e. as high as the values observed at 500 m depth during KEOPS rather than the 0.3 nM values used by Blain et al. (2007, 2008);
- (ii) our injection scheme for vertical iron supply, which adds more iron than the vertical diffusivity formulation;
- (iii) the flexible Fe/C stoichiometry in the model that reduces the DFe in the mixed layer to very low levels so that DFe input is large even in late winter and early spring when biomass is low.

In combination, these factors lead to much larger inputs for iron than for carbon, the model generating for the latter only  $\sim 2$  fold higher inputs from below ( $2.59 \text{ mol DIC m}^{-2} \text{ yr}^{-1}$  off-plateau and  $4.65 \text{ mol DIC m}^{-2} \text{ yr}^{-1}$  on plateau) in comparison to estimates based on the vertical diffusivity approach to budgets ( $0.58$  and  $1.22 \text{ mol DIC m}^{-2} \text{ yr}^{-1}$  for the HNLC and bloom, respectively; Jouandet et al., 2008).

The fate of iron in our model also differs from that estimated during KEOPS. In the model, 'new' Fe brought into the surface layer by the deepening of the mixed layer is taken up by phytoplankton. This iron ends up in a detrital

pool that is either regenerated into dissolved iron or exported out of the mixed layer. The export of detrital iron is an important sink, representing 45% of the uptake (while only 19% for carbon). This is higher than the 13% calculated for the SOIREE experiment (Bowie et al., 2001), and contrasts with the KEOPS seasonal budget, which retains iron more effectively than carbon within the mixed layer. The modelled daily export fluxes of iron outside the plateau were  $1700 \text{ nmol m}^{-2} \text{ d}^{-1}$  (maximum value), thus considerably higher than the  $458 \text{ nmol m}^{-2} \text{ d}^{-1}$  measured during the FeCycle experiment in subantarctic waters (Boyd et al., 2005; Frew et al., 2005), although the daily export flux as a fraction of the detrital standing stock of 0.09% in the model is similar to the FeCycle results.

In our model 38% of the iron being taken up by phytoplankton comes from regeneration within the mixed layer. This value is much lower than the one in the SOIREE experiment Fe budget of 83% (Bowie et al., 2001), and the general value of 86% computed by Fung et al. (2000) for the Southern Ocean. Overall in the model, the annual mixed-layer uptake ratio ( $\mu\text{mol-Fe/mol-DIC}$ ) is 42.6 outside the plateau and 272 inside (i.e. 6.4 times higher over the plateau). The equivalent ratios for the export fluxes are 98 (outside) and 584 (inside), (i.e. 6.0 times higher). The exported particles are thus slightly iron rich in the model in comparison to field measurements of 71–169 ( $\mu\text{mol-PFe/mol-POC}$ ) at the central bloom station A3 (Bowie, personal communication), again emphasizing the export of iron in comparison to carbon in the model. This emphasis on iron export is consistent with the effects of rescavenging of remineralized iron onto sinking particles (Clegg and Whitfield, 1990), although it reflects a different

parameterization in the model—i.e. luxury uptake of Fe along with the absence of a microbial loop for iron.

The carbon sequestration efficiency is a measure of the removal of carbon per unit iron provided. Methods for estimating an efficiency include (i) the ratio of DIC uptake to iron supply, (ii) the ratio of POC export to iron supply, and (iii) the ratio of ‘excess carbon export’ to ‘excess iron supply’ obtained by comparing iron-rich and iron-poor sites (De Baar et al., 2005). Table 1 provides a summary of these calculations. In our model, the DIC uptake/Fe supply inside the plateau of  $\sim 5522$  (mol/mol) is close to the average value of 5620 mol/mol calculated by De Baar et al. (2005) for artificial iron experiments. Outside the plateau, the efficiency is 10 times higher, at  $\sim 39,085$  mol/mol. Using the C export/Fe input diagnostic the model gives 9550 (mol/mol) outside and 1500 (mol/mol) inside. Using the carbon export in excess/Fe supply in excess we obtain a value of 703 (mol/mol), much lower than the 70,000 mol/mol calculated by Blain et al. (2007) or the 4300 (mol/mol) mean value for all the artificial iron experiments (De Baar et al., 2005).

The very low carbon sequestration efficiency in our model is driven by the high supply of iron and the flexible iron/carbon stoichiometry, which allows a strong uptake and export of iron with only a moderate carbon cycle response. While the magnitude of iron supply in our model is much larger than that estimated from the vertical eddy diffusivity by Blain et al. (2007), both approaches agree that the carbon sequestration efficiency is higher off the plateau than over it, meaning that the iron-limited HNLC ecosystem is more efficient at exporting carbon per unit Fe compared to the iron-replete ecosystem.

### 2.5. Sensitivity of the results to the rate of dispersion

We ran the two-dimensional the model using four values of the horizontal diffusion coefficient ( $K_y = 0, 250, 500,$  and  $1000 \text{ m}^2 \text{ s}^{-1}$ ). The impact of the increased dispersion on most terms of the carbon and iron budgets is rather small ( $\sim 20\%$  or less of the fluxes) compared to uncertainties about the vertical input of iron. However, the increased dispersion affects the carbon sequestration efficiency diagnostic somewhat more strongly off-plateau, (reducing the apparent efficiency nearly 2-fold). This is because the greater dispersion brings iron to the off-plateau region of the model and thus pushes the off-plateau C/Fe efficiency towards the low values that characterize the iron-replete system (as driven by the flexible Fe/C stoichiometry and high Fe export in the model).

## 3. Discussion

There are several aspects of the remote sensing observations that emphasize the over-simplifications of the model. The SCHL field is far from homogenous over the plateau, and shows higher values over regions of moderate bathymetry ( $\sim 650$  m depth) than in the shallowest areas

near seamounts or Heard Island. These may be areas of higher iron input as suggested by their correlations with elevated current velocities. Thus inhomogeneous, time-dependent iron inputs are probable, and may contribute to the phytoplankton response. Off the plateau, the SCHL field extends to the east in mid-summer, but its limits may be set not by a general dispersion of the iron (as parameterized in the model by a constant horizontal diffusivity) but by the interaction of the plateau with the ACC, which produces regions of rapid advection and dispersion in the meanders of the SAF to the northeast and in the Polar Front branches that cross the plateau near Kerguelen Island. Thus a hydrodynamic model is needed to further explore controls on bloom size and the fate of iron inputs from the Kerguelen plateau.

Our one-dimensional base model was calibrated for an open-ocean HNLC location (the KERFIX time series site to the west of Kerguelen). Simply increasing the iron-supply by a factor of 3 did a remarkably good job of simulating the phytoplankton bloom over the Kerguelen plateau in terms of its seasonal SCHL amplitude. These simulations were not perfect, especially in terms of the seasonal timing of the maximal biomass, which was approximately one month too late in comparison to the remote-sensing SCHL observations over the plateau. There are several ways in which the model could be improved, including hypothesizing earlier water-column stratification over the plateau and stronger response of phytoplankton growth rates to iron and/or light levels. However, without a seasonal cycle of observations this is not likely to be rewarding, especially given the considerable structure within the bloom, which probably includes variable seasonal cycles at individual locations, although the MODIS observations are too compromised by cloud cover to allow this to be determined with any clarity.

An important aspect of this study is that a model that permits flexible Fe/C stoichiometry leads to a relatively large loss of the enhanced iron input over the plateau in the form of iron-rich exported detritus. This then limits the influence of the plateau iron source on surrounding waters, and also leads to low carbon sequestration efficiency over the plateau. Interestingly, our model that estimates a high iron input (coupled to high iron export) provides similar nutrient depletion estimates to the field-based budgets by Blain et al. (2007) and Jouandet et al. (2008) that lead to high carbon sequestration efficiency based on low iron inputs (coupled to low iron export). Notably both approaches estimate a decrease in the carbon sequestration efficiency in the iron-replete bloom system in comparison to iron-poor HNLC system. Resolving the differences between these approaches requires improved understanding of how to calculate iron supply, and whether iron biogeochemistry in the Southern Ocean includes high Fe/C uptake ratios in late winter and early spring. The combined modelling and remote sensing approach presented here makes it clear that a full assessment of natural iron inputs on carbon sequestration also requires consideration of the

transfer of iron off the plateau and its effects on adjacent HNLC water masses.

#### 4. Conclusions

The phytoplankton bloom shape over the Kerguelen plateau clearly shows a relation with bathymetry and surface advection fields, but one that is much more complex than simply an increase of biomass in shallow waters. Further statistical analysis and the development of a hydrodynamic model are required to determine the detailed nature of this relation and especially the possible influence of topographic features and mixing characteristics on the transfer of iron to surface waters.

Using a simple model, we showed that the phytoplankton bloom over the plateau could be simulated using a model tailored to HNLC conditions in response to a 3-fold increase in subsurface iron concentrations. Physical dispersion moves some of the iron and associated biomass outside the plateau, but this is limited in extent by the high iron export that is parameterized in the model as a result of flexible Fe/C uptake stoichiometry. This may be an important process in limiting the influence of the iron inputs on surrounding waters. But more detailed analysis of the dispersion rate in and outside the plateau and more constraints on iron recycling in the Southern Ocean are needed to assess this further. By using simple techniques and tools we were able to highlight the main problems that hamper the assessment of the impact of iron fertilization on ocean carbon sequestration. The complexity of iron cycling, its interaction with complex hydrography of the Kerguelen plateau, and the heterogeneity of the SCHL distribution point to the need for new and specific tools to be developed to improve this assessment.

#### Acknowledgements

We thank Chris Rathbone for providing the MODIS AQUA images; Richard Coleman, Richard Matear, Heiner Dietze, and Andrew Bowie for their help during this project. This work was funded by the Australian Commonwealth Cooperative Research Centers Program through the Antarctic Climate and Ecosystems CRC. Tom Trull acknowledges support from LEGOS and the Observatoire midi-Pyrenees, Toulouse, France, during the completion of this work. Ernesto Molina acknowledges support from the University of Tasmania—CSIRO Marine and Atmospheric Research Quantitative Marine Science Ph.D. program.

#### References

Abraham, E.R., Law, C.S., Boyd, P.W., Lavender, S.J., Maldonado, M.T., Bowie, A., 2000. Importance of stirring in the development of an iron-fertilized phytoplankton bloom. *Nature* 407, 727–730.

Armand, L.K., Barthaux, V., Mosseri, J., Quéguiner, B., 2008. Late summer diatom biomass and community structure on and around the

naturally iron-fertilised Kerguelen Plateau in the Southern Ocean. *Deep-Sea Research II*, this issue [doi:10.1016/j.dsr2.2007.12.031].

Blain, S., Quéguiner, B., Armand, L., Belviso, S., Bombled, B., Bopp, L., Bowie, A., Brunet, C., Brussaard, C., Carlotti, F., Christaki, U., Corbière, A., Durand, I., Ebersbach, F., Fuda, J.-L., Garcia, N., Gerringa, L., Griffiths, B., Guigue, C., Guillermin, C., Jacquet, S., Jeandel, C., Laan, P., Lefèvre, D., Lomonaco, C., Malits, A., Mosseri, J., Obernosterer, I., Park, Y.-H., Picheral, M., Pondaven, P., Remy, T., Sandroni, V., Sarthou, G., Savoye, N., Scouarnec, L., Souhaut, M., Thuiller, D., Timmermans, K., Trull, T., Uitz, J., van-Beek, P., Veldhuis, M., Vincent, D., Viollier, E., Vong, L., Wagener, T., 2007. Effect of natural iron fertilisation on carbon sequestration in the Southern Ocean. *Nature* 446, 1070–1074.

Blain, S., Sarthou, G., Laan, P., 2008. Distribution of dissolved iron during the natural iron fertilization experiment KEOPS (Kerguelen plateau, Southern Ocean). *Deep-Sea Research II*, this issue [doi:10.1016/j.dsr2.2007.12.028].

Bowie, A.R., Maldonado, M.T., Frew, R.D., Croot, P.L., Achterberg, E.P., Mantoura, R.F.C., Worsfold, P.J., Law, C.S., Boyd, P.W., 2001. The fate of added iron during a mesoscale fertilisation in the Southern Ocean. *Deep-Sea Research II* 48, 2703–2744.

Boyd, P.W., et al., 2000. A mesoscale phytoplankton bloom in the polar Southern Ocean stimulated by iron fertilization. *Nature* 407, 695–702.

Boyd, P.W., Jackson, G.A., Waite, A.M., 2002. Are mesoscale perturbation experiments in Polar waters prone to physical artefacts? Evidence from algal aggregation modelling studies. *Geophysical Research Letters* 29 (11).

Boyd, P.W., et al., 2004. The decline and fate of an iron-induced subarctic phytoplankton bloom. *Nature* 428, 549–553.

Boyd, P.W., et al., 2005. FeCycle: attempting an iron biogeochemical budget from a mesoscale SF 6 tracer experiment in unperturbed low iron waters. *Global Biogeochemical Cycles*, 19 doi:10.1029/2005GB002494.

Carlotti, F., Thibault-Botha, D., Nowaczyk, A., Lefevre, D., 2008. Zooplankton community structure, biomass and role in carbon fluxes during the second half of a phytoplankton bloom in the eastern sector of the Kerguelen Shelf (January–February 2005). *Deep-Sea Research II*, this issue [doi:10.1016/j.dsr2.2007.12.010].

Clegg, S.L., Whitfield, M., 1990. A generalized model for the scavenging of trace metals in the open ocean–particle cycling. *Deep-Sea Research* 37, 809–832.

De Baar, H.J.W., Boyd, P., Coale, K., Tsuda, A., 2005. Synthesis of eight in situ iron fertilizations in high nutrient low chlorophyll waters confirms the control by wind mixed layer depth of phytoplankton blooms. *Journal of Geophysical Research* 110, 700–724.

Droop, M., 1974. The nutrient status of algal cell in continuous culture. *Journal of the Marine Biological Association of the United Kingdom* 54, 825–855.

Fiala, M., Kopczynska, E.E., Jeandel, C., Oriol, L., Vétion, G., 1998. Seasonal and interannual variability of size-fractionated phytoplankton biomass and community structure at station KERFIX, off the Kerguelen Island. *Journal of Plankton Research* 20 (7), 1341–1356.

Frew, R.D., Hutchins, D.A., Nodder, S., Sanudo-Wilhelmy, S., Tovar-Sanchez, A., Leblanc, K., Hare, C.E., Boyd, P.W., 2005. Particulate iron dynamics during FeCycle in subantarctic waters southeast of New Zealand. *Global Biogeochemical Cycles* 20.

Fung, I.Y., Meyn, S.K., Tegen, I., Doney, S.C., John, J.G., Bishop, J.K.B., 2000. Iron supply and demand in the upper ocean. *Global Biogeochemical Cycles* 19 (4), 20–32.

Gerringa, L.J.A., Blain, S., Laan, P., Sarthou, G., Veldhuis, M.J.W., Brussaard, C.P.D., Viollier, E., Timmermans, K.R., 2008. Fe-binding dissolved organic ligands near the Kerguelen Archipelago in the Southern Ocean (Indian sector). *Deep-Sea Research II*, this issue [doi:10.1016/j.dsr2.2007.12.007].

Jouandet, M.P., Blain, S., Metzl, N., Brunet, C., Trull, T.W., Obernosterer, I., 2008. A seasonal carbon budget for a naturally fertilized bloom over the Kerguelen plateau in the Southern Ocean. *Deep-Sea Research II*, this issue [doi:10.1016/j.dsr2.2007.12.037].

- Lancelot, C., Veth, C., Mathot, S., 1991. Modeling ice-edge phytoplankton bloom in the Scotia–Weddell Sea sector of the Southern Ocean during spring 1988. *Journal of Marine Systems* 2, 333–346.
- McCartney, M.S., Donohue, K.A., 2007. A deep cyclonic gyre in the Australian–Antarctic Basin. *Progress in Oceanography* 75 (4), 675–750.
- Mongin, M., Nelson, D.M., Pondaven, P., Tréguer, P., 2007. Potential phytoplankton responses to iron and stratification changes in the Southern Ocean based on a flexible-composition phytoplankton model. *Global Biogeochemical Cycles* 21 (GB4020), <<http://dx.doi.org/10.1029/2007GB002972>>.
- Mongin, M., Nelson, D., Pondaven, P., Brzezinski, M., Tréguer, P., 2003. Simulation of upper-ocean biogeochemistry with a flexible-composition phytoplankton model: C, N and Si cycling in the western Sargasso Sea. *Deep-Sea Research I* 50, 1445–1480.
- Mongin, M., Nelson, D.M., Pondaven, P., Tréguer, P., 2006. Simulation of upper-ocean biogeochemistry with a flexible-composition phytoplankton model: C, N and cycling and Fe limitation in the Southern Ocean. *Deep-Sea Research II* 53, 601–619.
- Moore, J.K., Abbott, M.R., 2000. Phytoplankton chlorophyll distributions and primary production in the Southern Ocean. *Journal of Geophysical Research* 105 (C12), 28709–28722.
- Moore, J.K., Abbott, M.R., 2002. Surface chlorophyll concentration in relation to the Antarctic Polar Front: seasonal and spatial patterns from satellite observation. *Journal of Marine Systems* 37, 69–86.
- Moore, J.K., Doney, S.C., Glover, D.M., Fung, I.Y., 2002. An intermediate complexity marine ecosystem model for the global domain. *Deep-Sea Research II* 49, 403–462.
- Mosseri, J., Quéguiner, B., Armand, L., Cornet-Barthaux, V., 2008. Impact of iron on silicon utilization by diatoms in the Southern Ocean: a case study of the Si/N cycle decoupling in a naturally iron-enriched area. *Deep-Sea Research II*, this issue [[doi:10.1016/j.dsr2.2007.12.003](https://doi.org/10.1016/j.dsr2.2007.12.003)].
- Obernosterer, I., Christaki, U., Lefèvre, D., Catala, P., Van Wambeke, F., Le Baron, P., 2008. Rapid bacterial remineralization of organic carbon produced during a phytoplankton bloom induced by natural iron fertilization in the Southern Ocean. *Deep-Sea Research II*, this issue [[doi:10.1016/j.dsr2.2007.12.005](https://doi.org/10.1016/j.dsr2.2007.12.005)].
- Park, Y.H., Fuda, J.L., Durand, I., Naveira Garabato, A.C., 2008a. Internal tides and vertical mixing over the Kerguelen plateau. *Deep-Sea Research II*, this issue [[doi:10.1016/j.dsr2.2007.12.027](https://doi.org/10.1016/j.dsr2.2007.12.027)].
- Park, Y.H., Roquet, F., Durand, I., Fuda, J.L., 2008b. Large scale circulation over and around the Northern Kerguelen plateau. *Deep-Sea Research II*, this issue [[doi:10.1016/j.dsr2.2007.12.030](https://doi.org/10.1016/j.dsr2.2007.12.030)].
- Pollard, R.T., Read, J.F., 2001. Circulation pathways and transports of the Southern Ocean in the vicinity of the Southwest Indian Ridge. *Journal of Geophysical Research* 106, 2881–2898.
- Pollard, R.T., Lucas, M.I., Read, J.F., 2002. Physical controls on biogeochemical zonation in the Southern Ocean. *Deep-Sea Research II* 49 (16), 3289–3305.
- Sarthou, G., Vincent, D., Christaki, U., Obernosterer, I., Timmermans, K.R., Brussaard, C.P.D., 2008. The fate of biogenic iron during a phytoplankton bloom induced by natural fertilization: impact of copepod grazing. *Deep-Sea Research II*, this issue [[doi:10.1016/j.dsr2.2007.12.033](https://doi.org/10.1016/j.dsr2.2007.12.033)].
- Savoie, N., Trull, T.W., Jacquet, S.H.M., Navez, J., Dehairs, F., 2008. <sup>234</sup>Th-based export fluxes during a natural iron fertilization experiment in the Southern Ocean. *Deep-Sea Research II*, this issue [[doi:10.1016/j.dsr2.2007.12.036](https://doi.org/10.1016/j.dsr2.2007.12.036)].
- Sokolov, S., Rintoul, S.R., 2007. On the relationship between fronts of the Antarctic Circumpolar Current and surface chlorophyll concentrations in the Southern Ocean. *Journal of Geophysical Research—Oceans* 112 (C07030).
- Stammer, D., 1998. Global characteristics of ocean variability estimated from regional TOPEX/POSEIDON altimeter measurements. *Journal of Physical Oceanography* 27, 1743–1769.
- Trull, T.W., Rintoul, S.R., Hadfield, M., Abraham, E.R., 2001a. Circulation and seasonal evolution of Polar waters south of Australia: implications for iron fertilization of the Southern Ocean. *Deep-Sea Research II* 48 (11–12), 2439–2466.
- Trull, T.W., Bray, S.G., Manganini, S.J., Honjo, S., François, R., 2001b. Moored sediment trap measurements of carbon export in the subantarctic and Polar Frontal Zones of the Southern Ocean, south of Australia. *Journal of Geophysical Research* 106 (C12), 31489–31510.
- Trull, T.W., Davies, D., Casciotti, K., 2008. Insights into nutrient assimilation and export in naturally iron-fertilized waters of the Southern Ocean from nitrogen, carbon and oxygen isotopes. *Deep-Sea Research II*, this issue [[doi:10.1016/j.dsr2.2007.12.035](https://doi.org/10.1016/j.dsr2.2007.12.035)].
- Van Beek, P., Bourquin, M., Reyss, J.L., Souhault, M., Charette, M.A., Jeandel, C., 2008. Radium isotopes to investigate the water mass pathways on the Kerguelen plateau (Southern Ocean). *Deep-Sea Research II*, this issue [[doi:10.1016/j.dsr2.2007.12.025](https://doi.org/10.1016/j.dsr2.2007.12.025)].
- Zhang, Y., Lacan, F., Jeandel, C., 2008. Dissolved rare earth elements tracing lithogenic inputs over the Kerguelen plateau (Southern Ocean). *Deep-Sea Research II*, this issue [[doi:10.1016/j.dsr2.2007.12.029](https://doi.org/10.1016/j.dsr2.2007.12.029)].